



Letter



Quantitatively relating multinucleon transfer and fusion

K.J. Cook^{a,b,*,} E.C. Simpson^a, D.C. Rafferty^a, D.J. Hinde^a, M. Dasgupta^a, J. Buete^a,
S.L. Hayles^a, L. Corradi^c, M. Evers^a, E. Fioretto^c, D.H. Luong^a, T. Mijatović^d, G. Montagnoli^e,
A.M. Stefanini^c, S. Szilner^d

^a Department of Nuclear Physics and Accelerator Applications, Research School of Physics, The Australian National University, Canberra, ACT 2601, Australia

^b Facility for Rare Isotope Beams, Michigan State University, MI 48824, USA

^c Istituto Nazionale di Fisica Nucleare, Laboratori Nazionali di Legnaro, I-35020 Legnaro, Italy

^d Ruđer Bošković Institute, Zagreb, Croatia

^e Dipartimento di Fisica e Astronomia, Università di Padova, via Marzolo 8, Padova, I-35131, Italy

ARTICLE INFO

Editor: B. Blank

Keywords:

Heavy-ion fusion

Capture

Multi-nucleon transfer

Energy dissipation

Fusion barrier-distribution

ABSTRACT

Above-barrier capture cross-sections for heavy ion-fusion are systematically lower than predictions, with the discrepancy rapidly growing with increasing charge product of the colliding nuclei. It has been proposed that this can be explained by the onset of energy dissipation *outside* the barrier. Here, we present measurements of both capture cross-sections and the reflected flux in the $^{32}\text{S}+^{208}\text{Pb}$ reaction to quantitatively correlate signatures of energy dissipation with the reduction of capture. The measurements of the reflected flux show that multinucleon transfer begins outside the barrier leading to high excitation energies and effective energy dissipation. We deduce the resulting change in kinetic energy relative to the new potential, and combine these with coupled channels calculations. This demonstrates that discrepancies between calculations and experimental cross-sections and barrier distributions can be quantitatively related to the observed multinucleon transfer.

1. Introduction

The fusion of two heavy nuclei is a challenge to our understanding of quantum many-body dynamics. Two many-body quantum systems having large numbers of degrees of freedom collide, interact, and merge, effectively irreversibly, into a single new compound nucleus. Given the complexity of the interactions, the short-range nucleon-nucleon interactions are represented by a mean-field attractive nuclear potential. When combined with the repulsive Coulomb potential, this produces a potential barrier to fusion. In quantum barrier-passing fusion models, fusion occurs only when the two colliding nuclei pass inside this barrier. Absorption (capture) inside the barrier is implemented mathematically via an incoming wave boundary condition or a short-range imaginary potential, neglecting the physical mechanism that leads to capture.

It has been long recognized that a single barrier-passing approach is unable to describe the observation of many orders of magnitude enhancement of fusion cross-sections below the barrier [1]. This phenomenon was addressed by treating the nuclei outside the barrier as being in a coherent quantum superposition of their ground state and

low-lying collective excited states, with coupling to a few transfer channels considered in an approximate manner [2,3]. This is the coupled-channels formalism (originally developed for scattering) and is currently the most successful type of model for heavy-ion fusion. The effect of the couplings is most clearly revealed in experimental barrier distributions [4], where couplings can be interpreted as causing a number of effective barriers to fusion [5].

However, there remains a long-standing problem: fusion cross-sections for heavy ion collisions are lower than the coupled-channels calculations at energies both above the barrier [6,7] and far below the barrier [8,6,9,10] when using a nuclear potential constrained by elastic scattering data [11,12]. The above-barrier fusion hindrance becomes substantially worse with increasing charge product between the projectile (P) and target (T) $Z_P Z_T$ [7], with experimental capture cross-sections being just $\sim 60\%$ of calculations by $Z_P Z_T \approx 1600$.

Proposed explanations for above- and below-barrier fusion hindrance can be separated into two types: dynamical and mean-field. In the latter, modifications are made to the shape (and thus inner turning point) of the potential, attributed to (for example) nuclear incom-

* Corresponding author at: Department of Nuclear Physics and Accelerator Applications, Research School of Physics, The Australian National University, Canberra, ACT 2601, Australia.

E-mail address: kaitlin.cook@anu.edu.au (K.J. Cook).

<https://doi.org/10.1016/j.physletb.2025.139465>

Received 9 December 2024; Received in revised form 4 April 2025; Accepted 8 April 2025

Available online 10 April 2025

0370-2693/© 2025 The Author(s). Published by Elsevier B.V. Funded by SCOAP³. This is an open access article under the CC BY license (<http://creativecommons.org/licenses/by/4.0/>).

pressibility [13,14] or the Pauli exclusion principle [15]. These act to widen the barrier, hindering tunneling and thus deep sub-barrier cross-sections. Additionally, if the process of capture is considered dynamically, the onset of energy damping may occur well *outside* the fusion barrier radius. Then, lower kinetic energies will result in reduced fusion cross-sections [6,16,7]. This proposed mechanism will reduce both above- and below-barrier fusion cross-sections [6].

Recently, measurements of the reflected flux in collisions of $^{40}\text{Ca} + ^{208}\text{Pb}$ have revealed that multinucleon transfer occurs with high probability outside the fusion barrier [17]. It was shown that multinucleon transfer can result in much-reduced kinetic energies with respect to the new barrier following transfer and hence reduced capture cross-sections. The observation of multinucleon transfer outside the barrier is consistent with previous measurements for more mass-symmetric systems [18,19].

Crucially, in Ref. [17], the fraction of reflected flux remaining as $^{40}\text{Ca} + ^{208}\text{Pb}$ was found to be only $11.6 \pm 0.1\%$ when the distance of closest approach was still 0.46 fm outside the single (uncoupled) barrier, with 31 different nuclide partitions comprising 95% of the reflected flux. The mean excitation energy of these many nuclide partitions was 19 MeV, expected to be largely in the heavy partner.

At such excitation energies, quantum states in nuclei are very dense and overlapping. The highly excited (doorway) state formed in transfer, as nuclei approach on the way to fusion, may be reasonably expected to evolve into the large number of overlapping states. This can occur for each partition. In heavy-ion reaction there can be tens of partitions even below the barrier [17], leading to extreme complexity. Evolution from doorway states populated following transfer to a large number of states is expected to cause (energy) dissipation [20,21].

The energy dissipation resulting from multinucleon transfer [22] on the path to fusion is similar to that of a compound nucleus, where the kinetic energy in the entrance channel is thermalised among many degrees of freedom. Thermalisation following multi-nucleon transfer on the incoming trajectory results in the energy not being available as kinetic energy on the timescale for fusion. This is the nature of the energy dissipation that we refer to in this paper.

In this Letter, we present two complementary measurements of $^{32}\text{S} + ^{208}\text{Pb}$ ($Z_p Z_T = 1472$) aimed to provide a quantitative understanding of the impact of multinucleon transfer on capture. We measure: (1) the capture cross-sections and deduce the fusion barrier distribution; (2) the energy dissipation in the reflected flux at below-barrier energies resulting from multinucleon transfer to high excitation energies. We empirically incorporate the measured change in kinetic energy (relative to the new barrier) resulting from excitation of the reaction products in multinucleon transfer with coupled-channels calculations. In doing so, we quantify the effect of the measured energy dissipation on both the fusion cross-sections and fusion barrier distribution.

2. Experimental methods

2.1. Reflected flux measurements with PRISMA

Measurements of the reflected flux of beam-like particles in collisions of $^{32}\text{S} + ^{208}\text{Pb}$ were performed at Legnaro National Laboratory XTU Tandem-ALPI accelerator complex, using the PRISMA magnetic spectrometer [23–25], located at $\theta_{lab} = 102^\circ$. PRISMA has a large solid angle (80 msr, $\Delta\theta_{lab} = \pm 6^\circ$, $\Delta\phi = \pm 11^\circ$), and momentum acceptance $\Delta p = \pm 10\%$, together with high mass-resolution $\Delta A/A \sim 1/200$, and energy resolution (via time-of-flight measurement) up to $1/1000$.

Beams of ^{32}S were delivered at 3 energies (with centre of mass energy $E_{c.m.} = 140.9, 153.1$ and 165.2 MeV) onto $\sim 150 \mu\text{g}/\text{cm}^2$ ^{208}PbS targets oriented with their normals at 60° to the beam axis. The $E_{c.m.}$ have been corrected for energy loss through the half-target thickness. The targets had $20 \mu\text{g}/\text{cm}^2$ carbon backings which were oriented upstream such that the particles accepted into PRISMA did not pass through the carbon backing. Reactions from the carbon and sulfur components of the target

are in inverse kinematics, and therefore were forward focused and did not enter PRISMA at $\theta_{lab} = 102^\circ$.

Absolute probabilities of the integrated reflected flux $P_{\text{reflected}}$ were determined by normalising to $^{32}\text{S} + ^{208}\text{Pb}$ Rutherford scattering yields in two Si beam monitoring detectors placed at forward angles on either side of the beam axis. To approximately account for the transmission probability through PRISMA [26], it was assumed that at the lowest energy (where reactions are expected to be purely quasielastic), $d\sigma_{\text{reflected}}/d\sigma_{\text{Rutherford}} = P_{\text{reflected}} = 1$.

The atomic number Z , mass number A and kinetic energy of the reflected beam-like particles accepted into PRISMA were determined through measurement of their energy loss ΔE , magnetic rigidity $B\rho$ and time-of flight (TOF) [23]. The ions passed through a position-sensitive microchannel plate timing detector (MCP) [27] before traversing a quadrupole and dipole magnet. Subsequently, the ions passed through a multi-wire parallel-plate avalanche counter (MWPPAC) then into a segmented ionisation chamber at the focal plane [28]. The positions of the ions measured in the MCP and MWPPAC defined the trajectory of the ions through the magnetic elements, determining the magnetic rigidity $B\rho$. The energy loss of ions in the ionisation chamber enabled the determination of Z , and in combination with $B\rho$, the charge-state q . Together with time-of-flight (TOF), this allowed determination of A (and hence neutron number $N = A - Z$) and the kinetic energy of the projectile-like nuclei.

The determination of excitation energy allows the *explicit* determination of the change in kinetic energy of each event with respect to the new potential barrier following transfer [17]. This key step in the analysis allows us to calculate the effect of energy dissipation on fusion barrier distributions and cross-sections, discussed in detail in Sec. 3.2. The reaction Q-value and hence excitation energy E_x was reconstructed for each event using two-body kinematics. We estimate the E_x resolution of PRISMA in this analysis to be ~ 2 MeV FWHM.

2.2. Capture cross-sections & barrier distribution measurements with CUBE

In $^{32}\text{S} + ^{208}\text{Pb}$ reactions, capture leads almost exclusively to fusion-fission or quasifission, so measurement of fission fragments allows determination of capture cross-sections σ . The measurement of precise capture cross-sections in small energy steps enables the determination of the experimental barrier distribution $d^2 E\sigma/dE^2$. As the capture cross-sections (though not the barrier distribution) from this measurement were published previously [29], the measurement will be only briefly summarised.

Pulsed beams of ^{32}S in the energy range $E_{lab} = 151.7$ to 211.8 MeV were delivered by the Heavy Ion Accelerator Facility at the Australian National University. The beams impinged on ^{208}PbS ($> 99\%$ enrichment) targets of thicknesses ranging from 25 to $90 \mu\text{g}/\text{cm}^2$ evaporated onto $15 \mu\text{g}/\text{cm}^2$ C backings, which faced downstream. Fission fragments were detected in coincidence using the large-acceptance CUBE multi-wire proportional counter (MWPC) detector array [30,31]. Two beam monitor detectors (Si) were placed at forward angles above and below the beam axis to enable absolute cross-section normalisation using Rutherford scattering. Solid angle calibration of the CUBE detectors was achieved by simultaneously measuring elastic scattering in the MWPCs and in the monitor detectors at deep sub-barrier energies. The known folding angle of elastic-recoil coincidences enabled checking of the geometrical calibration, achieving agreement to $\pm 0.1^\circ$.

The fission fragment angular distributions were determined for each energy at centre-of-mass angles between 120° and 170° . The total fission cross-sections were extracted by fitting these angular distributions using the transition state model, treating K_0^2 as a free parameter as described in Refs. [32,33].

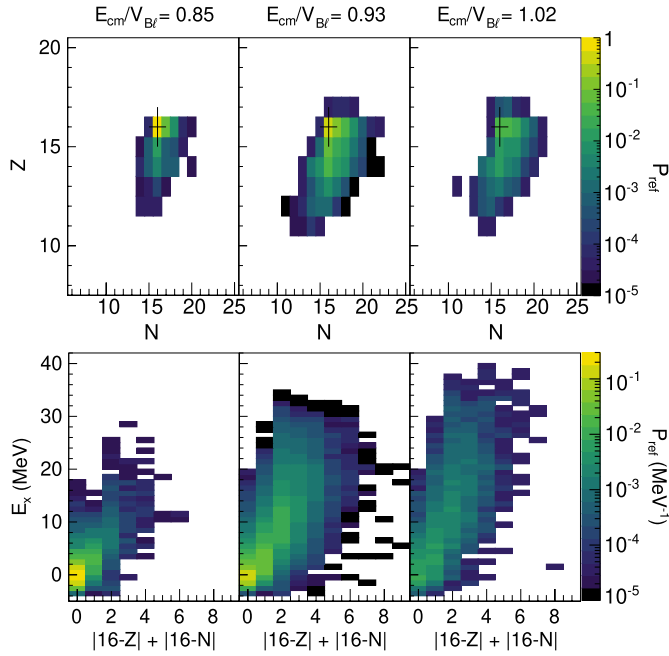


Fig. 1. Top: The N, Z distribution of the reflected flux measured at $\theta_{lab} = 102^\circ$ in the $^{32}\text{S} + ^{208}\text{Pb}$ reaction for the three energies measured. Each column is labelled by the beam energy with respect to its ℓ -dependent fusion barrier calculated for $\theta_{lab} = 102^\circ$. The cross indicates the location of the projectile nuclide ^{32}S (in)elastic channel. Bottom: Excitation energy as a function of the minimum number of transferred nucleons for each energy, determined by the net number nucleons transferred from the entrance channel $|16 - Z| + |16 - N|$.

3. Results and discussion

3.1. Reflected flux N, Z, E_x distribution

The N, Z distributions from the measurements with PRISMA (Sec. 2.1) are shown in top row of Fig. 1 for the three measured energies. The colour scale shows the absolute probability of a nuclide being in the outgoing (reflected) trajectory following the collision of $^{32}\text{S} + ^{208}\text{Pb}$. Immediately below each N, Z distribution is the excitation energy of the nuclei in the reflected flux as a function of the number of nucleons away from the elastic channel $|16 - Z| + |16 - N|$. As multinucleon transfer will involve the transfer of nucleons both towards and away from the projectile, this quantity is a measure of the *minimum* number of transferred nucleons.

Since the measurement was made at a fixed angle of 102° ($\Delta\theta_{lab} = \pm 6^\circ$), each measurement probes only a small range of ℓ . The ℓ corresponding to that for Rutherford trajectories scattering to $\theta_{lab} = 102^\circ$, are $\ell = 63, 60, 58$ in order of increasing beam energy. Thus, each column in Fig. 1 is labelled with $E/V_{B\ell}$, the beam energy with respect to the ℓ -dependent fusion barrier (where the nuclear potential parameters used were that of the inert barrier calculation in Sec. 3.3.1).

As the energy increases, the fraction of the reflected flux remaining as $^{32}\text{S} + ^{208}\text{Pb}$ (at the position of the cross in each panel) decreases, and the excitation energy broadens and increases. While few nucleon transfer and inelastic scattering largely contribute to the total flux (as also seen in [34]), multinucleon transfer produces a very broad range of N, Z , having high excitation energies. Even well below the barrier at $E/V_{B\ell} = 0.93$, 49 different nuclide pairs are observed in the reflected flux, well beyond what would be expected from (in)elastic and few nucleon transfer, consistent with the onset of deep-inelastic processes and with observations from measurements of $^{40}\text{Ca} + ^{208}\text{Pb}$ [17]. Importantly, even in significantly improved calculations [35], this degree of complexity – the number of nuclide pairs and extent of excitation energy – is not captured.

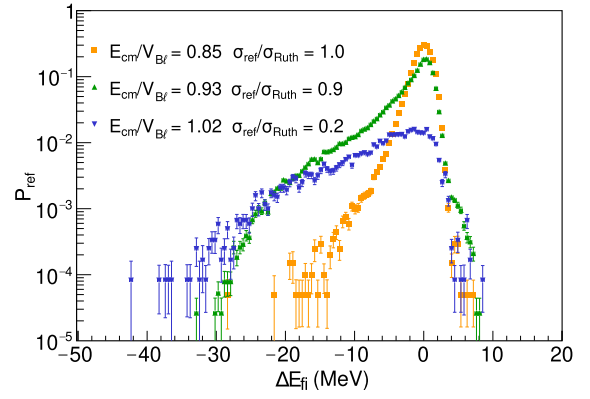


Fig. 2. Distribution of kinetic energy of the reflected flux with respect to the new internuclear potential ΔE_{fi} following transfer in reactions of $^{32}\text{S} + ^{208}\text{Pb}$ at $\theta_{lab} = 102^\circ$ for three beam energies $E/V_{B\ell} = 0.85, 0.93, 1.02$. The integrated reflected flux probabilities compared to Rutherford scattering $\sigma_{ref}/\sigma_{Ruth}$ are indicated.

The measured N, Z, E_x distributions depend on the acceptance of PRISMA. The magnetic fields of PRISMA were set for each energy to maximise the transmission of the dominant charge state of the elastically scattered beam. Binary reaction channels outside the PRISMA acceptance of $\Delta p \pm 10\%$ – those with large changes in N, Z or energy – would not be transmitted to the focal plane. Our measurements are thus lower limits of the distributions of N, Z , and so likely also of dissipated energy. Capture outcomes for $^{32}\text{S} + ^{208}\text{Pb}$ are known to produce slow quasifission and fusion-fission with masses near mass-symmetry [36], well outside the acceptance of PRISMA in these measurements, so the observed distributions cannot have a significant component of events associated with re-separation following capture.

3.2. Energy dissipation in the reflected flux

The integrated impact of multinucleon transfer on fusion can be determined by evaluating a new variable ΔE_{fi} measuring the change in kinetic energy relative to the new internuclear potential following transfer ΔE_{fi} [17]. ΔE_{fi} is calculated under the assumption that transfer occurs at the distance of closest approach R_{min} and is given by

$$\Delta E_{fi} = [E' - V'(R_{min})] - [E - V(R_{min})], \quad (1)$$

where E and E' are the kinetic energies and V and V' are the Coulomb potentials at R_{min} in the initial and final states, respectively. This is equivalent to,

$$\Delta E_{fi} = Q_{gg} - E_x - [V'(R_{min}) - V(R_{min})] \quad (2)$$

where Q_{gg} is the ground-state to ground-state Q-value and E_x is the excitation energy.

Events with $\Delta E_{fi} > 0$ mean that following transfer there is an increase in kinetic energy relative to the (new) potential which should increase capture. Conversely, $\Delta E_{fi} < 0$ decreases the kinetic energy relative to the new internuclear potential, reducing capture. We note that $V'(R_{min}) - V(R_{min})$ approximates the optimum Q-value [37–40], where there is a smooth joining of trajectories in the entrance and exit channels. Therefore, ΔE_{fi} represents a measure of how much each event deviates from the optimum Q-value.

The ΔE_{fi} distributions for the reflected flux measured in $^{32}\text{S} + ^{208}\text{Pb}$ reactions are shown in Fig. 2. At the lowest measured energy, the distribution peaks strongly at $\Delta E_{fi} = 0$, predominantly arising from elastic scattering with $E_x = 0$ MeV and no change in the internuclear potential. The peak remains at $E/V_{B\ell} = 0.93$, having additional strong contributions from transfers that lead to excitation energies at the optimum Q-value. The peak is hardly present for $E/V_{B\ell} = 1.02$, likely due to a com-

bination of capture and through multinucleon transfer moving events to more negative ΔE_{fi} .

At higher energies, a strong, nearly exponentially decreasing tail tending towards negative ΔE_{fi} forms, hardly changing between $E/V_{B\ell} = 0.93$ and $E/V_{B\ell} = 1.02$. The tail extending to negative ΔE_{fi} has two origins [17]: the exponential increase in the density of states with increasing E_x , causing an enhancement of transfer probabilities towards the high E_x (more negative ΔE_{fi}) side of the optimum Q-value, and multiple nucleon transfers in both directions (deep-inelastic scattering) leading to high excitation energies [41,42]. As discussed in the introduction, these high excitation energies lead to energy dissipation due to high level densities. Thus, the nuclei have less kinetic energy available to overcome the potential barrier.

We are faced with two seemingly opposing facts: (1) that barrier passing models provide a reasonable reproduction of fusion cross-sections, when they assume that colliding nuclei are essentially unchanged in N , Z , and E_x before capture; (2) that by the time the barrier is reached, the colliding nuclei have exchanged significant mass, charge and are in a wide range of excited states. The fact that ΔE_{fi} shows a peak at 0 MeV provides a resolution: since the kinetic energy of the colliding nuclei remain largely unchanged *with respect to their new barrier*, then the transmission coefficients are similar, resulting in similar cross-sections. Simultaneously, the amount of flux located at negative ΔE_{fi} , and thus decreased energy with respect to the new barrier, provides a mechanism for effective energy dissipation, hindering fusion at above-barrier energies. This idea can be tested via empirical inclusion of the distribution of ΔE_{fi} on barrier passing calculations.

3.3. Fusion cross-sections and barrier distribution

The capture barrier distribution for $^{32}\text{S}+^{208}\text{Pb}$, the second derivative of the energy weighted capture cross-sections, was extracted [5] using the point-difference formula with energy steps of ~ 2.5 MeV, and is shown in Fig. 3(a) and (b). The experimental barrier distribution has a mean value of 145.2 MeV, with a wide distribution and attenuated peak structure. The measured capture cross-sections are shown in Fig. 3(c), the uncertainties are typically $< 1\%$ and smaller than the size of the points.

3.3.1. Coupled-channels calculations

Coupled-channels calculations for the fusion of $^{32}\text{S}+^{208}\text{Pb}$ were performed using the CCFULL code [43]. Three representative results are shown by the dashed lines in Fig. 3. In all cases, the Woods-Saxon potential parameters were taken to be $r_0 = 1.05$ fm, $a_0 = 0.70$ fm from the systematic analysis of Ref. [7], while the depth parameter V_0 was adjusted in each calculation to reproduce the centroid of the barrier distribution. The magenta dashed line shows the calculated inert (no-couplings are included) barrier distribution, scaled by 0.5 to fit on the graph. As would be expected, this calculation does not reproduce the width or structure in the measured barrier distribution.

The next calculations follow the ‘standard’ approach by including the lowest-energy collective excitations in the projectile and target as they have the maximum effect on the barrier distribution. Including one-phonon harmonic vibrational couplings of states in both the projectile and target, being 2^+ ($E_x = 2.23$ MeV, $\beta_2 = 0.314$) for ^{32}S [44], and for ^{208}Pb , 3^- ($E_x = 2.615$ MeV, $\beta_3 = 0.111$) and 5^- ($E_x = 3.198$ MeV, $\beta_5 = 0.061$) [45] is shown by the dashed green line in Fig. 3(a). It provides a better reproduction of the width of the barrier distribution, but the peak of the experimental barrier distribution at 144 MeV coincides with a dip in the calculation. The comparison is improved when two-phonon harmonic couplings of the same states are included, as shown in the dashed blue line in Fig. 3(b). The barrier distribution is smoother than the one-phonon calculation and the width of the calculated barrier distribution approximately coincides with the experiment. The peaks in the calculated barrier distribution approximately agree with the location of increased strength of the experimental barrier distribution, but

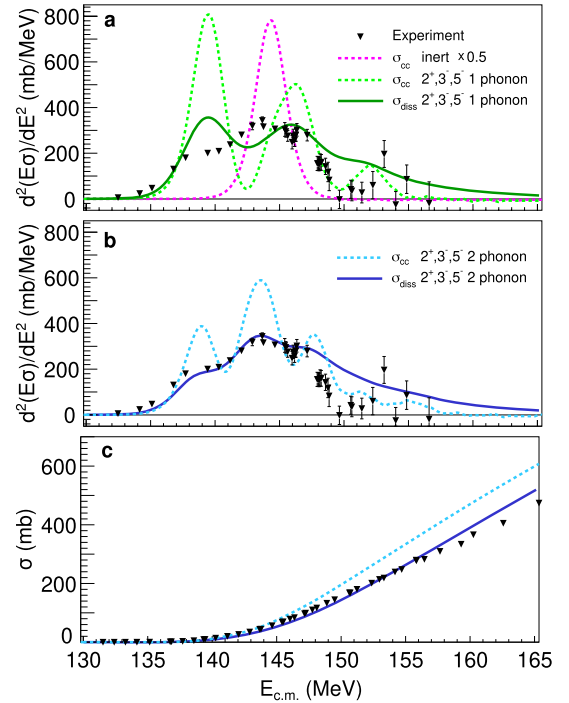


Fig. 3. (a) Measured $^{32}\text{S}+^{208}\text{Pb}$ barrier distribution with energy steps of ~ 2.5 MeV (black triangles), compared to coupled-channels (CCFULL) calculations σ_{cc} , described in the text. The dashed magenta line shows the calculated inert barrier distribution (scaled by 0.5 to preserve the y-axis). The green dashed line shows the calculation assuming single-phonon couplings to the first 2^+ state in ^{32}S and the first 3^- and 5^- states in ^{208}Pb . The green solid line shows the ‘dissipated’ barrier distribution σ_{diss} , obtained by folding the calculated σ_{cc} (green dashed) with the distribution of reflected kinetic energies with respect to the barrier ΔE_{fi} . (b) Same as for (a), but with calculations showing two-phonon couplings of the same state. (c) Measured $^{32}\text{S}+^{208}\text{Pb}$ capture cross-sections (black), compared to the two-phonon coupled channels calculation (dashed blue) and the folded ‘dissipated’ fusion cross-section (solid dark blue). The statistical error bars of the experimental cross-sections are smaller than the points.

still show too much amplitude. All mutual couplings (including mutual excitations) were included in the coupling scheme, though this had little impact on the results. Adding two-neutron transfer ($Q_{gg} = 5.953$ MeV, $F_{tr} = 0.3$) had similarly minor effects on the barrier distribution. Adding more and/or higher-order couplings [46] should modify the barrier distribution, but the full spectroscopic data to perform these calculations is not available.

The measured above-barrier capture cross-sections for $^{32}\text{S}+^{208}\text{Pb}$ shown in Fig. 3(c) are $\sim 25\%$ lower than the two-phonon coupled-channels calculations (blue dashed line), consistent with the systematic study of Ref. [7]. Given that $^{32}\text{S}+^{208}\text{Pb}$ approaches the barrier in a multitude of different (N,Z) pairs with large changes in kinetic energy, it is no surprise that the coupled channels calculation with a limited number of channels fails to reproduce the experimental data.

3.4. Impact of multinucleon transfer on cross-sections

The measurement of the change in kinetic energy relative to the new potential ΔE_{fi} shown in Fig. 2 allows quantitative evaluation of the impact of multinucleon transfer on the calculated cross-sections. We construct a ‘dissipated’ fusion cross-section $\sigma_{diss}(E_{c.m.})$, that models the colliding nuclei at a given initial energy $E_{c.m.}$ as experiencing a range of kinetic energies $E_{c.m.} + \Delta E_{fi}$ due to multinucleon transfer leading to energy dissipation, as defined above. The probability distribution of kinetic energies is given by $P(\Delta E_{fi}, E_{c.m.})$, and the cross-sections for each $E_{c.m.} + \Delta E_{fi}$ are taken from the coupled-channels calculations σ_{cc} , giving:

$$\sigma_{diss}(E_{c.m.}) = \sum_{\Delta E_{fi}} P(\Delta E_{fi}, E_{c.m.}) \sigma_{cc}(E_{c.m.} + \Delta E_{fi}). \quad (3)$$

In principle, the $P(\Delta E_{fi}, E_{c.m.})$ distribution will evolve with $E_{c.m.}$ and needs to be that for all possible trajectories – those that fuse and those that lead to other outcomes. This is naturally a very difficult quantity to determine experimentally. We are therefore forced to make a simplifying assumption and use a constant $P(\Delta E_{fi})$ distribution. We take the conservative choice, using $P(\Delta E_{fi})$ measured at $E/V_{B\ell} = 0.93$. Here, multinucleon transfer has begun, producing the tail in ΔE_{fi} , but little absorption has occurred ($\sigma_{reflected}/\sigma_{Rutherford} = 0.91$) to impact the shape of the measured multinucleon transfer distribution. It was seen in ref [17] for $^{40}\text{Ca} + ^{208}\text{Pb}$ that the shape of the tail of ΔE_{fi} hardly changes from $E/V_{B\ell} = 0.91$ to $E/V_{B\ell} = 0.99$, meaning that choosing $E/V_{B\ell} = 0.93$ may be expected to reasonably represent the multinucleon transfer in this small energy region, though it might be expected to evolve above the barrier (discussed below). To account for the small effect of absorption, we normalise $P(\Delta E_{fi})$ such that $\int P(\Delta E_{fi}) dE_{fi} = 1$.

Using this procedure to take energy dissipation into account, the fusion cross-sections σ_{diss} and associated barrier distributions are shown by the full blue lines in [Fig. 3(b,c)], calculated using the same two-phonon coupled channels calculation as before. The fusion cross-sections with dissipation included empirically are in excellent agreement with the experimental data up to 155 MeV, but are increasingly above the experiment at higher energies. The corresponding barrier distribution is lowered and spread, significantly improving the agreement with the experimental data while producing a tail of probability extending to high energies. The much better correspondence between these calculations and the experimental data indicates that the measured N, Z, E_x distributions of multinucleon transfer outside the fusion barrier is consistent with the observed suppression of fusion compared to standard calculations.

The use of the measured reflected flux at below barrier energies and single θ relies on the assumption that this accurately represents the $P(\Delta E_{fi}, E_{c.m.})$ at each ℓ that leads to capture. Since σ_{cap} at a given $E_{c.m.}$ is largely determined by the limiting ℓ for fusion, measuring $P(\Delta E_{fi}, E_{c.m.})$ as a function of ℓ (i.e. varying $\theta_{c.m.}$ at below-barrier energies) is an important avenue for future work.

The overestimation of the cross-sections above 155 MeV and the high-energy tail of barrier strength are likely caused by the assumption that $P(\Delta E_{fi}, E_{c.m.})$ for all values of energy and ℓ is represented by that measured at $E/V_{B\ell} = 0.93$ for one scattering angle. It is expected that as $E_{c.m.}$ increases, the limiting ℓ for capture increases, and thus the matter overlap also increases. This results in more nucleon exchange and evolution towards more negative ΔE_{fi} compared to that at $E/V_{B\ell} = 0.93$, decreasing the available kinetic energy even more, and further suppressing the cross-sections. As a further complication, the measured reflected flux will have components arising from multinucleon transfer occurring both before and after the distance of closest approach, when only the processes occurring on the incoming trajectories are relevant to fusion. Further investigations of low-energy multinucleon transfer and so the evolution of ΔE_{fi} with energy and angle is necessary. In the much heavier system $^{206}\text{Pb} + ^{118}\text{Sn}$, very recent results show very long tails of total kinetic energy loss (TKEL), with increasing yields with energy [47]. A theoretical approach to this problem is very attractive, as the calculation of accurate multinucleon transfer cross-sections and energy distributions would alleviate many of the above assumptions imposed by experiment. The semi-classical model GRAZING [48] reproduces the low excitation energy portion of multinucleon transfer very well. However, it systematically fails (see for example, Fig. 2. of ref. [47]) to reproduce the large tail of high excitation energies leading to energy dissipation, which act to lower and spread the barrier distributions. Further theoretical developments will be necessary.

The present approach, of taking measured transfer distributions and combining these with coupled-channels calculations has similarities with Ref. [35], where the transfer form-factors are modified to reflect the measured Q-value distribution. However, in Ref. [35], only specific

few-nucleon transfer channels are included (though many more than in standard CCFULL) and all couplings are assumed to remain coherent. In contrast, here we treat all changes in kinetic energy with respect to the new barrier as irreversible on the timescale of fusion. In reality, there will be a smooth evolution from full coherence to dissipative energy loss as the system becomes more complex with increasing level density. Since thermalisation is correlated with level density, the excitation energy at which thermalisation occurs will be higher for collisions of light nuclei than for heavy nuclei, potentially explaining why above-barrier capture suppression decreases with decreasing charge-product [7].

3.5. Remaining signatures of channel couplings

In the calculation of σ_{diss} it is implicit that the channel couplings for all the mass partitions are well-represented by those for $^{32}\text{S} + ^{208}\text{Pb}$. This may be questioned – a majority of the collisions change their N, Z partition prior to reaching the fusion barrier, as seen in Fig. 1. However, the correspondence between the experimental and CCFULL barrier distributions in Fig. 3(b) seem to suggest that the nature of the low-lying couplings included in the calculation remain important.

To illustrate this, the green magenta line Fig. 3(a) shows the σ_{diss} obtained using the single-phonon coupling scheme. This results in a σ_{diss} barrier distribution that is much too wide, with too much strength in the lower and higher parts of the barrier distribution.

How can the structure of the original colliding nuclei remain relevant to the barrier distribution after multiple transfers? Collective states of nuclei result from the many constituent nucleons, and are initially excited through the long-range Coulomb interaction. Since the energy and strength of collective states generally vary slowly with nucleon number, we expect that the transfer of a small number of nucleons will not substantially change the collective motion of the whole nucleus. For example, ^{32}S has a first 2^+ with $E_x = 2.23$ MeV $\beta_2 = 0.314$, while for ^{30}Si ($-2p$) $E_x = 2.23$ MeV and $\beta_2 = 0.330$, almost identical. Similarly for the target-like nucleus, while the first 3^- state in ^{208}Pb has $E_x = 2.615$ MeV, $\beta_3 = 0.111$, ^{210}Po (the complementary fragment to ^{30}Si) has its first 3^- state at $E_x = 2.39$ MeV, $\beta_3 = 0.109$. Similar behaviour is seen in the 3^- states in Pb isotopes. One might therefore expect that the structure of the barrier distribution arising from collective couplings for $^{30}\text{Si} + ^{210}\text{Po}$ to be similar to that for $^{32}\text{S} + ^{208}\text{Pb}$. Structure in the barrier distribution will therefore remain provided that following transfer, a major part of the flux couples to similar low-lying collective states as the entrance channel. Whilst currently, the exact nature of the couplings and the evolution of multinucleon transfer distributions is not known, it is clear that for a full understanding of heavy-ion fusion, a quantitative treatment of both coherent coupling to low-lying states and multinucleon transfer leading to non-zero ΔE_{fi} and energy dissipation is necessary to reproduce the measured barrier distribution.

4. Conclusions

For heavy-ion reactions with large charge products $Z_1 Z_2 > 500$, a consistent reproduction of observables cannot be achieved using a single mean-field potential. Discrepancies are found in:

1. above- and below-barrier capture cross-sections, which cannot be reproduced simultaneously [6],
2. the shape of the fusion barrier distributions do not agree [49],
3. fusion and quasi-elastic scattering cross-sections, which require very different potential diffuseness parameters [11,50].

The capture cross-sections of $^{32}\text{S} + ^{208}\text{Pb}$ presented here fit into this longstanding picture – showing a lower above-barrier cross-section compared to coupled-channels calculations, and a barrier distribution that cannot be reproduced by including only couplings to low-lying collective states.

We address this discrepancy by making measurements of the N , Z , and E_x of reflected flux in sub-barrier reactions of $^{32}\text{S}+^{208}\text{Pb}$ at $\theta_{lab} = 102^\circ$. These showed that substantial multinucleon transfer begins at energies well below the (ℓ -dependent) fusion barrier, indicating that it can occur prior to capture. Wide ranges of N , Z are populated, often leading to high excitation energies. This may well explain why calculations assuming that $^{32}\text{S}+^{208}\text{Pb}$ collide essentially unchanged in N , Z fail to reproduce the data.

In order to quantitatively determine the influence of multinucleon transfer on fusion, we combined the distributions of N , Z and E_x following multinucleon transfer into a single quantity, the change in kinetic energy of the colliding nuclei with respect to their (new) barrier. We find that:

1. The distribution of the change in kinetic energy ΔE_{fi} shows a long tail of lowered kinetic energies relative to their new potential due to multinucleon transfer leading to high excitation energies, consistent with energy dissipation. This will hinder fusion.
2. After folding the calculated fusion cross-sections from coupled channels calculations with the measured ΔE_{fi} distribution at $E/V_{B\ell} = 0.93$, where multinucleon transfer has begun but little absorption has occurred, the resulting deduced cross-sections and barrier distributions are in much better agreement with experimental measurements.

This result was obtained assuming that ΔE_{fi} does not evolve with energy or angular momentum, and that the transfer products experience the same couplings to collective states as in the entrance channel ($^{32}\text{S}+^{208}\text{Pb}$). Even better agreement may be obtained by including these effects once they can be quantified from further measurements. The details of the impact of multinucleon transfer on the barrier distribution and capture cross-sections will depend on the precise form of the ΔE_{fi} distribution. However, multinucleon transfer will always produce an excitation energy distribution with some portion of events having high excitation energy. This means that multinucleon transfer (when present) will act to reduce above-barrier capture cross-sections and smooth barrier distributions though some signatures of channel couplings remain.

Declaration of competing interest

The authors declare that they have no known competing financial interests or personal relationships that could have appeared to influence the work reported in this paper.

Acknowledgements

This work was supported by Australian Research Council Grants DP190101442, DP200100601, DE230100197 and DP230101028. T.M. and S.S. acknowledge the support of the Croatian Science Foundation under Project no. 7194 and Project no. IP-2018-01-1257. The authors acknowledge the facilities, and the scientific and technical assistance provided by Heavy Ion Accelerators (HIA). HIA is supported by the Australian Government through the National Collaborative Research Infrastructure Strategy (NCRIS) program. The efforts of the accelerator staff at the INFN Legnaro National Laboratory are gratefully acknowledged.

Data availability

Data will be made available on request.

References

- [1] M. Beckerman, Sub-barrier fusion of two nuclei, Rep. Prog. Phys. 51 (8) (1988) 1047, <https://doi.org/10.1088/0034-4885/51/8/001>.
- [2] C. Dasso, S. Landowne, A. Winther, Channel-coupling effects in heavy-ion fusion reactions, Nucl. Phys. A 405 (2) (1983) 381–396, [https://doi.org/10.1016/0375-9474\(83\)90578-X](https://doi.org/10.1016/0375-9474(83)90578-X).
- [3] K. Hagino, K. Ogata, A. Moro, Coupled-channels calculations for nuclear reactions: from exotic nuclei to superheavy elements, Prog. Part. Nucl. Phys. 125 (2022) 103951, <https://doi.org/10.1016/j.pnpnp.2022.103951>.
- [4] N. Rowley, G. Satchler, P. Stelson, On the “distribution of barriers” interpretation of heavy-ion fusion, Phys. Lett. B 254 (1) (1991) 25–29, [https://doi.org/10.1016/0370-2693\(91\)90389-8](https://doi.org/10.1016/0370-2693(91)90389-8).
- [5] M. Dasgupta, D.J. Hinde, N. Rowley, A.M. Stefanini, Measuring barriers to fusion, Annu. Rev. Nucl. Part. Sci. 48 (1) (1998) 401–461, <https://doi.org/10.1146/annurev.nucl.48.1.401>.
- [6] M. Dasgupta, D.J. Hinde, A. Diaz-Torres, B. Bouriquet, C.I. Low, G.J. Milburn, J.O. Newton, Beyond the coherent coupled channels description of nuclear fusion, Phys. Rev. Lett. 99 (2007) 192701, <https://doi.org/10.1103/PhysRevLett.99.192701>.
- [7] J.O. Newton, R.D. Butt, M. Dasgupta, D.J. Hinde, I.I. Gontchar, C.R. Morton, K. Hagino, Systematic failure of the Woods-Saxon nuclear potential to describe both fusion and elastic scattering: possible need for a new dynamical approach to fusion, Phys. Rev. C 70 (2004) 024605, <https://doi.org/10.1103/PhysRevC.70.024605>.
- [8] H. Esbensen, C.L. Jiang, A.M. Stefanini, Hindrance in the fusion of $^{48}\text{Ca}+^{48}\text{Ca}$, Phys. Rev. C 82 (2010) 054621, <https://doi.org/10.1103/PhysRevC.82.054621>.
- [9] C.L. Jiang, K.E. Rehm, B.B. Back, R.V.F. Janssens, Survey of heavy-ion fusion hindrance for lighter systems, Phys. Rev. C 79 (2009) 044601, <https://doi.org/10.1103/PhysRevC.79.044601>.
- [10] H. Esbensen, S. Mişicu, Hindrance of $^{16}\text{O}+^{208}\text{Pb}$ fusion at extreme sub-barrier energies, Phys. Rev. C 76 (2007) 054609, <https://doi.org/10.1103/PhysRevC.76.054609>.
- [11] A. Mukherjee, D.J. Hinde, M. Dasgupta, K. Hagino, J.O. Newton, R.D. Butt, Failure of the Woods-Saxon nuclear potential to simultaneously reproduce precise fusion and elastic scattering measurements, Phys. Rev. C 75 (2007) 044608, <https://doi.org/10.1103/PhysRevC.75.044608>.
- [12] M. Evers, M. Dasgupta, D.J. Hinde, L.R. Gasques, M.L. Brown, R. Rafiei, R.G. Thomas, Systematic study of the nuclear potential diffuseness through high precision back-angle quasi-elastic scattering, Phys. Rev. C 78 (2008) 034614, <https://doi.org/10.1103/PhysRevC.78.034614>.
- [13] S. Mişicu, H. Esbensen, Hindrance of heavy-ion fusion due to nuclear incompressibility, Phys. Rev. Lett. 96 (2006) 112701, <https://doi.org/10.1103/PhysRevLett.96.112701>.
- [14] S. Mişicu, H. Esbensen, Signature of shallow potentials in deep sub-barrier fusion reactions, Phys. Rev. C 75 (2007) 034606, <https://doi.org/10.1103/PhysRevC.75.034606>.
- [15] C. Simenel, A.S. Umar, K. Godbey, M. Dasgupta, D.J. Hinde, How the Pauli exclusion principle affects fusion of atomic nuclei, Phys. Rev. C 95 (2017) 031601, <https://doi.org/10.1103/PhysRevC.95.031601>.
- [16] K. Hagino, Evolving theoretical descriptions of heavy-ion fusion: from phenomenological to microscopic approaches, EPJ Web Conf. 163 (2017) 00022, <https://doi.org/10.1051/epjconf/201716300022>.
- [17] K.J. Cook, D.C. Rafferty, D.J. Hinde, E.C. Simpson, M. Dasgupta, L. Corradi, M. Evers, E. Fioretto, D. Jeung, N. Lobanov, D.H. Luong, T. Mijatović, G. Montagnoli, A.M. Stefanini, S. Szilner, Colliding heavy nuclei take multiple identities on the path to fusion, Nat. Commun. 14 (1) (2023), <https://doi.org/10.1038/s41467-023-43817-8>.
- [18] F.L.H. Wolfs, Fission and deep-inelastic scattering yields for $^{58}\text{Ni}+^{112,124}\text{Sn}$ at energies around the barrier, Phys. Rev. C 36 (1987) 1379–1386, <https://doi.org/10.1103/PhysRevC.36.1379>.
- [19] J. Gehring, B.B. Back, K.C. Chan, M. Freer, D. Henderson, C.L. Jiang, K.E. Rehm, J.P. Schiffer, M. Wolanski, A.H. Wuosmaa, Deep-inelastic scattering in $^{124,136}\text{Xe}+^{58,64}\text{Ni}$ at energies near the Coulomb barrier, Phys. Rev. C 55 (1997) 2959–2964, <https://doi.org/10.1103/PhysRevC.55.2959>.
- [20] K. Hagino, N. Takigawa, Effects of finite width of excited states on heavy-ion sub-barrier fusion reactions, Phys. Rev. C 58 (1998) 2872–2878, <https://doi.org/10.1103/PhysRevC.58.2872>.
- [21] A. Balantekin, N. Takigawa, Path integral approach to multidimensional quantum tunnelling, Ann. Phys. 160 (2) (1985) 441–476, [https://doi.org/10.1016/0003-4916\(85\)90152-6](https://doi.org/10.1016/0003-4916(85)90152-6).
- [22] D.Y. Jeung, D.J. Hinde, E. Williams, M. Dasgupta, E.C. Simpson, R. du Rietz, D.H. Luong, R. Rafiei, M. Evers, I.P. Carter, K. Ramachandran, C. Palshetkar, D.C. Rafferty, C. Simenel, A. Wakhle, Energy dissipation and suppression of capture cross sections in heavy ion reactions, Phys. Rev. C 103 (2021) 034603, <https://doi.org/10.1103/PhysRevC.103.034603>.
- [23] A. Stefanini, L. Corradi, G. Maron, A. Pisent, M. Trotta, A. Vinodkumar, S. Beghini, G. Montagnoli, F. Scarlassara, G. Segato, A. De Rosa, G. Inglima, D. Pierroutsakou, M. Romoli, M. Sandoli, G. Pollarolo, A. Latina, The heavy-ion magnetic spectrometer prisma, in: 5th International Conference on Radioactive Nuclear Beams, Nucl. Phys. A 701 (1) (2002) 217–221, [https://doi.org/10.1016/S0375-9474\(01\)01578-0](https://doi.org/10.1016/S0375-9474(01)01578-0).
- [24] S. Szilner, C.A. Ur, L. Corradi, N. Märginean, G. Pollarolo, A.M. Stefanini, S. Beghini, B.R. Behera, E. Fioretto, A. Gadea, B. Guiot, A. Latina, P. Mason, G. Montagnoli, F. Scarlassara, M. Trotta, G.d. Angelis, F.D. Vedova, E. Farnea, F. Haas, S. Lenzi, S. Lunardi, R. Märginean, R. Menegazzo, D.R. Napoli, M. Nespolo, I.V. Pokrovsky, F. Recchia, M. Romoli, M.-D. Salsac, N. Soić, J.J. Valiente-Dobón, Multinucleon transfer reactions in closed-shell nuclei, Phys. Rev. C 76 (2007) 024604.

- [25] L. Corradi, S. Szilner, G. Pollarolo, D. Montanari, E. Fioretto, A. Stefanini, J. Valiente-Dobón, E. Farnea, C. Michelagnoli, G. Montagnoli, F. Scarlassara, C. Ur, T. Mijatović, D. Jelavić Malenica, N. Soić, F. Haas, Multinucleon transfer reactions: present status and perspectives, in: XVIIth International Conference on Electromagnetic Isotope Separators and Techniques Related to Their Applications, December 2–7, 2012 at Matsue, Japan, Nucl. Instrum. Methods Phys. Res., Sect. B, Beam Interact. Mater. Atoms 317 (2013) 743–751.
- [26] D. Montanari, E. Farnea, S. Leoni, G. Pollarolo, L. Corradi, G. Benzoni, A. Gadea, E. Fioretto, A. Latina, G. Montagnoli, F. Scarlassara, A.M. Stefanini, S. Szilner, Response function of the magnetic spectrometer prisma, Eur. Phys. J. A 47 (2011) 1–7, <https://doi.org/10.1140/epja/i2011-11004-9>.
- [27] G. Montagnoli, A. Stefanini, M. Trotta, S. Beghini, M. Bettini, F. Scarlassara, V. Schiavon, L. Corradi, B. Behera, E. Fioretto, A. Gadea, A. Latina, S. Szilner, L. Donà, M. Rigato, N. Kondratiev, A.Y. Chizhov, G. Kniajeva, E. Kozulin, I. Pokrovskiy, V. Voskressensky, D. Ackermann, The large-area micro-channel plate entrance detector of the heavy-ion magnetic spectrometer prisma, Nucl. Instrum. Methods Phys. Res., Sect. A, Accel. Spectrom. Detect. Assoc. Equip. 547 (2) (2005) 455–463, <https://doi.org/10.1016/j.nima.2005.03.158>.
- [28] S. Beghini, L. Corradi, E. Fioretto, A. Gadea, A. Latina, G. Montagnoli, F. Scarlassara, A. Stefanini, S. Szilner, M. Trotta, A. Vinodkumar, The focal plane detector of the magnetic spectrometer prisma, Nucl. Instrum. Methods Phys. Res., Sect. A, Accel. Spectrom. Detect. Assoc. Equip. 551 (2) (2005) 364–374, <https://doi.org/10.1016/j.nima.2005.06.058>.
- [29] D.J. Hinde, M. Dasgupta, N. Herrald, R.G. Neilson, J.O. Newton, M.A. Lane, Isotopic dependence of fusion barrier energies in reactions forming heavy elements, Phys. Rev. C 75 (2007) 054603, <https://doi.org/10.1103/PhysRevC.75.054603>.
- [30] D.J. Hinde, M. Dasgupta, J.R. Leigh, J.C. Mein, C.R. Morton, J.O. Newton, H. Timmers, Conclusive evidence for the influence of nuclear orientation on quasifission, Phys. Rev. C 53 (1996) 1290–1300, <https://doi.org/10.1103/PhysRevC.53.1290>.
- [31] R. du Rietz, E. Williams, D.J. Hinde, M. Dasgupta, M. Evers, C.J. Lin, D.H. Luong, C. Simenel, A. Wakhle, Mapping quasifission characteristics and timescales in heavy element formation reactions, Phys. Rev. C 88 (2013) 054618, <https://doi.org/10.1103/PhysRevC.88.054618>.
- [32] D. Hinde, C. Morton, M. Dasgupta, J. Leigh, J. Mein, H. Timmers, Competition between fusion-fission and quasi-fission in the reaction $^{28}\text{Si} + ^{208}\text{Pb}$, Nucl. Phys. A 592 (2) (1995) 271–289, [https://doi.org/10.1016/0375-9474\(95\)00306-L](https://doi.org/10.1016/0375-9474(95)00306-L).
- [33] D.J. Hinde, A.C. Berriman, M. Dasgupta, J.R. Leigh, J.C. Mein, C.R. Morton, J.O. Newton, Limiting angular momentum for statistical model description of fission, Phys. Rev. C 60 (1999) 054602, <https://doi.org/10.1103/PhysRevC.60.054602>.
- [34] L. Corradi, A.M. Stefanini, D. Ackermann, S. Beghini, G. Montagnoli, C. Petrache, F. Scarlassara, C.H. Dasso, G. Pollarolo, A. Winther, Multinucleon transfer reactions in $^{32}\text{S} + ^{208}\text{Pb}$ close to the Coulomb barrier, Phys. Rev. C 49 (1994) R2875–R2879, <https://doi.org/10.1103/PhysRevC.49.R2875>.
- [35] G. Colucci, E. Piasecki, A. Trzcińska, P.W. Wen, V. Palmin, T. Abramova, Dissipation by transfer and its influence on barrier distributions, Phys. Rev. C 109 (2024) 064625, <https://doi.org/10.1103/PhysRevC.109.064625>.
- [36] J. Khuyagbaatar, D.J. Hinde, I.P. Carter, M. Dasgupta, C.E. Düllmann, M. Evers, D.H. Luong, R. du Rietz, A. Wakhle, E. Williams, A. Yakushev, Experimental study of the quasifission, fusion-fission, and de-excitation of cf compound nuclei, Phys. Rev. C 91 (2015) 054608, <https://doi.org/10.1103/PhysRevC.91.054608>.
- [37] J. Schiffer, H. Körner, R. Siemssen, K. Jones, A. Schwarzschild, Experimental study of angular distributions and optimum q values in heavy-ion reactions, Phys. Lett. B 44 (1) (1973) 47–49, [https://doi.org/10.1016/0370-2693\(73\)90297-9](https://doi.org/10.1016/0370-2693(73)90297-9).
- [38] J. Wilczyński, Optimum Q-value in multinucleon transfer reactions, Phys. Lett. B 47 (2) (1973) 124–128, [https://doi.org/10.1016/0370-2693\(73\)90586-8](https://doi.org/10.1016/0370-2693(73)90586-8).
- [39] L. Corradi, G. Pollarolo, S. Szilner, Multinucleon transfer processes in heavy-ion reactions, J. Phys. G, Nucl. Part. Phys. 36 (11) (2009) 113101, <https://doi.org/10.1088/0954-3899/36/11/113101>.
- [40] D. Brink, Kinematical effects in heavy-ion reactions, Phys. Lett. B 40 (1) (1972) 37–40.
- [41] K.E. Rehm, A.M. van den Berg, J.J. Kolata, D.G. Kovar, W. Kutschera, G. Rosner, G.S.F. Stephens, J.L. Yntema, Transition from quasi-elastic to deep-inelastic reactions in the $^{48}\text{Ti} + ^{208}\text{Pb}$ system, Phys. Rev. C 37 (1988) 2629–2646, <https://doi.org/10.1103/PhysRevC.37.2629>.
- [42] J. Randrup, Theory of transfer-induced transport in nuclear collisions, Nucl. Phys. A 327 (2) (1979) 490–516, [https://doi.org/10.1016/0375-9474\(79\)90271-9](https://doi.org/10.1016/0375-9474(79)90271-9).
- [43] K. Hagino, N. Rowley, A. Kruppa, A program for coupled-channel calculations with all order couplings for heavy-ion fusion reactions, Comput. Phys. Commun. 123 (1) (1999) 143–152, [https://doi.org/10.1016/S0010-4655\(99\)00243-X](https://doi.org/10.1016/S0010-4655(99)00243-X).
- [44] J. Chen, ^{32}S , Nucl. Data Sheets 201 (1) (2025).
- [45] M. Martin, ^{208}Pb , Nucl. Data Sheets 108 (1583) (2007).
- [46] J.M. Yao, K. Hagino, Anharmonicity of multi-octupole-phonon excitations in ^{208}Pb : analysis with multireference covariant density functional theory and subbarrier fusion of $^{16}\text{O} + ^{208}\text{Pb}$, Phys. Rev. C 94 (2016) 011303, <https://doi.org/10.1103/PhysRevC.94.011303>, <https://link.aps.org/doi/10.1103/PhysRevC.94.011303>.
- [47] S. Szilner, L. Corradi, J. Diklič, T. Mijatović, F. Galtarossa, G. Pollarolo, E. Fioretto, A. Goasduff, G. Montagnoli, A.M. Stefanini, G. Colucci, P. Čolović, A. Gottardo, J. Grebosz, A. Illana, G. Jaworski, M.J. Gomez, T. Marchi, D. Mengoni, M. Milin, D. Nurkić, M. Siciliano, N. Soić, D. Testov, J.J. Valiente-Dobón, N. Vukman, Quest for cooper pair transfer in heavy-ion reactions: the $^{206}\text{Pb} + ^{118}\text{Sn}$ case, Phys. Rev. Lett. 133 (2024) 202501, <https://doi.org/10.1103/PhysRevLett.133.202501>.
- [48] A. Winther, Grazing reactions in collisions between heavy nuclei, Nucl. Phys. A 572 (1) (1994) 191–235, [https://doi.org/10.1016/0375-9474\(94\)90430-8](https://doi.org/10.1016/0375-9474(94)90430-8).
- [49] E. Piasecki, L. Świdorski, N. Keeley, M. Kisieliński, M. Kowalczyk, S. Khlebnikov, T. Krogulski, K. Piasecki, G. Tiourin, M. Sillanpää, W.H. Trzaska, A. Trzcińska, Smoothing of structure in the fusion and quasielastic barrier distributions for the $^{20}\text{Ne} + ^{208}\text{Pb}$ system, Phys. Rev. C 85 (2012) 054608, <https://doi.org/10.1103/PhysRevC.85.054608>.
- [50] L.R. Gasques, M. Evers, D.J. Hinde, M. Dasgupta, P.R.S. Gomes, R.M. Anjos, M.L. Brown, M.D. Rodríguez, R.G. Thomas, K. Hagino, Systematic study of the nuclear potential through high precision back-angle quasi-elastic scattering measurements, Phys. Rev. C 76 (2007) 024612, <https://doi.org/10.1103/PhysRevC.76.024612>, <https://link.aps.org/doi/10.1103/PhysRevC.76.024612>.